A theoretical proposal of high performance blood components biosensor based on defective 1D photonic crystal employing WS$_2$, MoS$_2$ and graphene

Abinash Panda[1] · **Puspa Devi Pukhrambam**[1]

Abstract

In this research, a novel configuration of 1D photonic crystal (PhC) is proposed for the detection of numerous elements present in human blood such as plasma, RBC, biotin, serum albumin. The proposed structure is envisaged with an alternate arrangement of CaF$_2$, PtSe$_2$ and ZnSe with a central defect layer, where the wall of the defect layer is separately coated with novel 2D materials like WS$_2$, MoS$_2$ and graphene to enhance the sensor performance. The well-known transfer matrix method (TMM) is employed to compute the transmission spectrum and absorption spectrum by infiltrating the defect layer with blood components. The cornerstone of this work is to observe the shift in the defect mode wavelength in the transmission spectrum. The geometrical parameters of the structure such as thickness of dielectric layers, defect layer, refractive index of dielectric layers and the number of period are judiciously optimized to realize effective sensor. The effect of variation in the defect layer thickness and angle of incidence on the transmission spectrum is thoroughly studied. Additionally, the number of layers of WS$_2$, MoS$_2$ and graphene are suitably optimized for design of high performance biosensor. Various sensing characteristics such as sensitivity, signal-to-noise ratio (SNR), quality factor (QF), figure of merit (FOM), resolution and detection limit (DL) are evaluated and compared for the proposed WS$_2$, MoS$_2$ and graphene based sensor configurations. Moreover, the simple structure, cost-effective fabrication methods and label-free detection of blood components make the proposed sensor a promising challenger for biosensing applications.

✉ Abinash Panda
  abinashpanda087@gmail.com

[1] Department of Electronics and Communication Engineering, National Institute of Technology, Silchar, Assam 788010, India

1 Introduction

Photonic crystal structures (PhCs) were first introduced by E. Yablonovitch and S. John in early 1987, which brought a revolution in the research domain of photonics by exploring an array of novel applications (Yablonovitch 1987; John 1987; Elsayed 2018; Abd El-Aziz et al. 2019a). The PhCs are the special class of artificial arrangements, which are envisaged as the periodic organization of low and high refractive index materials (Devashish et al. 2019; Ahmed and Mehaney 2019). Among the various PhCs configurations (1D/2D/3D), 1D structures have experienced a significant rise in demand owing to their simple structural arrangement, low loss, cost-effective fabrication techniques, compatibility with photonic integrated circuits, and extensive application area (Panda and Devi 2020; Panda et al. 2018). When electromagnetic (EM) waves are interacted with PhCs, a distinctive property is perceived known as photonic band gap (PBG), where light of certain frequency ranges are prohibited to pass through the structure (Ghasemi et al. 2019; Entezar et al. 2015). The properties of PBG are strongly influenced by the nature of applied material such as semiconductor, metamaterial, metal, plasma, superconductor, nano-composite materials etc. (Aly and Sayed 2020; Shi et al. 2001). A defect can be realised in a perfect PhC by breaking its periodicity via altering the geometrical properties of a layer, introducing a different material into the structure or exterminating a layer from the structure (Boedecker and Henkel 2003; Hattori 2002). When the incident light frequency matches with the defect mode frequency, the photons are positioned within the band gap, which forms a resonant peak (Ghasemi et al. 2019; Hemmatyar et al. 2017). The position and intensity of these resonant peaks are varied with nature of dielectric materials, nature of defect layer, thickness of the defect layer.

Over the last decade, 1D PhC structures have been extensively employed for various bio-sensing applications. Aly et al. (2020a) reported a defect based 1D PhC with a sensitivity of 306.25 nm RIU^{-1} to detect various concentrations of creatinine present in the blood. Jahania et al. (2020) studied the defective PhC structure with inclusion of graphene sheets for biochemical sensing application in terahertz regime. A highly sensitive alcohol sensor is presented (Shaban et al. 2020) to detect different concentrations of ethanol, methanol and propanol by employing the transfer matrix method. Bouzidi et al. (2017) investigated the shifts in the reflectance spectrum of a defect based PhC structure with respect to various glucose concentrations in blood. The reference (Abd El-Aziz et al. 2019b) proposed a defected 1D PhC biosensor for sensing protein concentrations, where the authors analysed the effect of defect layer thickness on the sensitivity. However, the authors found a maximum sensitivity of only 170 nm per RIU. Nouman et al. (2020) inspected the shift in resonant wavelength in a defect based 1D PhC for detection of brain lesions in a very small time. A 2D PhC with line defect is proposed (Sharma et al. 2014) to detect different blood components using FDTD (finite domain time difference) approach. A PhC ring resonator structure is reported in the wavelength range 1530–1615 nm for sensing various blood components, where the authors obtained a quality factor of 262 and detection limit of 0.002 RIU^{-1} (Arunkumar et al. 2019). Mohammad et al. (2019) studied a 2D PhC with nanocavity to sense numerous blood components. But in the references (Sharma et al. 2014; Arunkumar et al. 2019; Mohammed et al. 2019), the proposed structures are relatively complex and difficult to fabricate with high accuracy.

The performance of 1D PhC structure can be greatly enhanced by using novel materials like graphene, WS_2 and MoS_2. So, we have included these 2D materials in our design, to enhance the sensing performance. Graphene has received enormous attention on

electromagnetic applications owing to its unmatched attributes, for instance, robustness, high mobility, one atom thickness, flexibility, durability, extraordinary optical, thermal and electrical conductivity at room temperature, frequency-independent absorption of EM radiation (Falkovsky and Pershoguba 2007; Geim 2009; Bonaccorso et al. 2010). Graphene has emerged as a suitable candidate for superb conductive support for nanoparticles to realize hybrid nanocomposites (Liu, 2018; Wei, 2017; Zang, 2017). The conductivity of graphene can be regulated over a wide frequency range by changing the chemical potential across the graphene sheets, which can appositely alter the optical properties of photonic structures integrated with graphene. The coating of graphene can significantly increase the sensitivity to change in refractive index. A sort of 2D materials such as WS_2 and MoS_2, which belong to the Transition metal dichalcogenides (TMD) group, have attracted a substantial research attention owing to their scalability property, and thickness dependent optical properties. WS_2 and MoS_2 has large band gap of 1.94 eV and 1.77 eV respectively, which is higher than the conventional semiconductor materials, thus make them feasible to manage a high temperature and voltage. With a broad work function of 5.1 eV, MoS_2 offers high affinity surface area to absorb the bio-analytes and thus utilized in bio-sensing applications (Kukkar et al. 2016). WS_2 comprises a hexagonal crystal structure and shows a higher 2nd order nonlinear susceptibility and broad frequency response (Janisch, 2015). Moreover, the high photoluminescence, nonblinking photon emission, wider PBG (visible to near-infrared wavelength range) and large surface area of WS_2, high spin orbit coupling of 420 meV, makes it a favourable material to realize biosensors (Yuan and Huang 2015; Zhu et al. 2015). Recently, $PtSe_2$ has evolved as a gifted material for various optoelectronic applications, owing to its unmatched electrical and optical properties, and adjustable bandgap in the range 1.2 eV to 0.21 eV (Wang, 2015). In addition to this, $PtSe_2$ is highly inertness towards various chemical agents and shows good resistant to toxic effect, which makes it a suitable candidate for bio sensing applications (Jia et al. 2020).

Blood is the most important aspect of human body, as it runs the oxygen and food to each corner of the body. Blood cells are consisted of a verity of components like red blood cell (RBC), white blood cell (WBC), pallets, biotin, plasma etc. The blood appears to be red color because of presence of RBC in it, whereas the liquid part of the blood is plasma. Biotins are constituted with various types of vitamin and pallets are made up of bone marrow and help in clotting of blood. Any disorder in the blood flow in body may incur numerous diseases like lymphoma, myeloma, leukemia, anemia, malaria, haemophilia. So, it is indispensable to correctly and timely detect various concentrations of blood components to avoid any chance of fatality. Nevertheless, different methods of blood tests are available like kombo test, blood smear, blood count, bone marrow biopsy, flame atomic absorption spectroscopy (Wolf and Zitelli 1987), but these tests are time consuming and require more blood samples and sophisticated laboratory facilities. Optical bio-sensing technique can be an apposite alternative for the analysis of different blood components as this method requires small amount of blood samples for detection and provides accurate results in less time. Mainly, two types of optical methods can be applied to test blood components such as fluorescent technique and label-free detection technique. As it is quite challenging to perform quantitative analysis of blood components using fluorescent technique, so the label-free detection technique is widely used by the research community. In label-free detection technique, refractive index of blood components plays the most vital role to analyse the sample (Boyd and Heebner 2001; White and Fan 2008). The refractive index based label-free detection method greatly simplifies the sensing process by reducing the time, effort and experimental artefacts. Apart from this, the refractive index based sensors are extensively studied and practically employed for a broad bio-sensing applications (Aly et al.

2020a; Jahania et al. 2020; Shaban et al. 2020; Bouzidi et al. 2017; Abd El-Aziz et al. 2019b; Nouman et al. 2020; Sharma et al. 2014; Arunkumar et al. 2019; Mohammed et al. 2019).

This research proposes label-free detection of various blood components such as water, plasma, RBC, biotin and serum albumin having refractive index of 1.330, 1.350, 1.400, 1.450 and 1.470 respectively (Sharma et al. 2014; Arunkumar et al. 2019; Mohammed et al. 2019). For this purpose, a defect based 1D PhC structure is employed, which includes completely new combination of dielectric materials CaF_2, $PtSe_2$ and ZnSe along with other novel 2D materials like MoS_2, WS_2 and graphene. To the best of author's knowledge, first time we have proposed such kind of novel 1D structures to realize high performance blood components sensor. Different geometrical parameters like thickness of dielectric layers, thickness of defect layer, thickness of 2D materials, period of the dielectric layers, incident angle are properly optimized, which add another feather of novelty to this work. Both transmission and absorption spectrum are investigated here, which is not found in any of the research listed in the literature. Aside from this, a complete set of performance measuring parameters such as sensitivity, signal-to-noise ratio (SNR), quality factor (QF), figure of merit (FOM), resolution (R), detection limit (DL) are computed. Moreover, with the available simple and cost effective fabrication methodologies, the authors believe that the proposed sensor can bring a remarkable advancement in the biosensing applications.

2 Proposed model and method

In this communication, a central defect based 1D PhC with the periodic arrangement of CaF_2, $PtSe_2$ and ZnSe is investigated, which is shown in Fig. 1. The motivation for selecting these materials is their large refractive index difference and feeble absorption in the considered wavelength range. A defect is created at the centre, which is infiltrated with blood as the analyte to detect its various components. The sidewalls of the defect layer (D) are separately coated with novel 2D materials like graphene, MoS_2 and WS_2 to efficiently
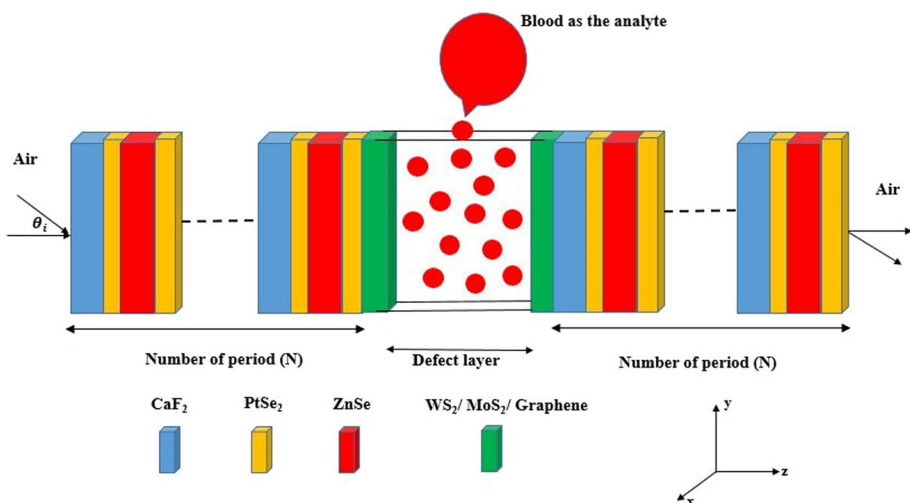

Fig. 1 Schematic view of the proposed 1D PhC sensor

absorb the analytes. Herewith, we have assayed three different multilayer configurations such as $(CaF_2/PtSe_2/ZnSe)^N$(graphene/D/graphene)$(CaF_2/PtSe_2/ZnSe)^N$,$(CaF_2/PtSe_2/ZnSe)^N$(WS$_2$/D/WS$_2$)$(CaF_2/PtSe_2/ZnSe)^N$ and $(CaF_2/PtSe_2/ZnSe)^N$(MoS$_2$/D/MoS$_2$)$(CaF_2/PtSe_2/ZnSe)^N$. The period (N) of the aforementioned structures is selected as N=5. A He–Ne laser source is used to generate a light of wavelength 632.8 nm, which incidents on the proposed structure. The refractive index of CaF$_2$ and ZnSe is taken as $n_{CaF_2} = 1.432$ and $n_{ZnSe} = 2.578$, whereas their thickness are chosen as $d_{CaF_2} = d_{ZnSe} = 300$ nm. We also analysed the transmittance spectrum for higher values of d_{CaF_2} and d_{ZnSe}, but we found that for higher thickness values, the resonant modes are more broadened and show high FWHM, which is undesired. Refractive index of PtSe$_2$ is selected as $n_{PtSe_2} = 3.016 + 1.673 * i$ at a thickness of $d_{PtSe_2} = 6$ nm (Guo 2020). At the considered wavelength of 632.8 nm, refractive index of graphene is considered as $3 + 1.149 * i$ (Han 2019; Keshavarz et al. 2020). Similarly, refractive index of MoS$_2$ and WS$_2$ is computed as $n_{MoS2} = 5.08 + 1.172 * i$ and $n_{WS_2} = 4.9 + 0.312 * i$ respectively at 632.8 nm (Han 2019; Keshavarz et al. 2020). Thickness of graphene, MoS$_2$ and WS$_2$ is selected as 0.34*L nm, 0.65*L nm and 0.80*L nm respectively, where L signifies the number of layers (Han 2019; Keshavarz et al. 2020). The transfer matrix method (TMM) is manipulated to study the transmittance spectrum of the proposed structure for various blood components at defect layer thicknesses (d_D) of 400 nm and 500 nm.

With a tremendous advancement in technology, the authors are confident that the proposed 1D structure can be easily fabricated. Different layers of dielectric materials like CaF$_2$ and ZnSe can be precisely fabricated on a glass substrate by several accepted methods such as sol–gel method (Ilinykh and Matyushkin 2016), magnetron sputtering (Schürmann et al. 2006), spin coating (Wang et al. 2008), and chemical vapour deposition (CVD) (Chen et al. 2008). Moreover, recently Zahid et al. (2020) and Mittal et al. (2017) experimentally fabricated a thin film of CaF$_2$ and ZnSe. Apart from this Qi et al. (2018), reported the detail fabrication process for realization of various 2D TMDs materials like graphene, MoS$_2$ and WS$_2$, PtSe$_2$ by using different methods like physical vapour transport (PVT), molecular beam epitaxy (MBE), chemical vapour deposition (CVD), and mechanical exfoliation. With the aforementioned fabrication techniques, the authors believe that it is feasible to realize the proposed sensor.

3 Mathematical analysis

Transfer matrix method (TMM) is employed for effective analysis of band gap characteristics through computation of transmission spectra of the proposed layered 1D PhC (Aly et al. 2020a; Abd El-Aziz et al. 2019b). Each layer is represented in the form of its own matrix and the overall transfer matrix of the entire structure is computed through multiplication of all the discrete layer matrices. As shown in Fig. 1, the EM waves incident on the proposed structure at angle θ_i and propagate along the x direction, which confirm that the electric fields (E_m) and magnetic fields (H_m) propagate in y–z plane. The electric field and magnetic field in air i.e. E_0 and H_0 can be computed by solving the following matrix equation,

$$\begin{bmatrix} E_0 \\ H_0 \end{bmatrix} = M_1, M_2, M_3, \ldots M_N \begin{bmatrix} E_m \\ H_m \end{bmatrix} \tag{1}$$

where N represents the total number of layers with inclusion of the defect layer, M specifies the characteristics matrix. The characteristics matrix of the pth layer can be expressed as,

$$M_p = \begin{bmatrix} cos\delta_p & \left(-\dfrac{i}{\varphi_p}\right)sin\delta_p \\ -i\varphi_p sin\delta_p & cos\delta_p \end{bmatrix} \tag{2}$$

where

$$\delta_p = \frac{2\pi}{\lambda}d_p n_p cos\theta_p \tag{3}$$

where λ denotes the incident wavelength, n_p is the refractive index and d_p is the thickness of the pth layer. Here, θ_p is the incident angle in the pth layer. Further, φ_p can be written as,

$$\varphi_p = \sqrt{\frac{\varepsilon_0}{\mu_0}}n_p cos\theta_p \quad \text{for TE mode} \tag{4a}$$

$$\varphi_p = \sqrt{\frac{\varepsilon_0}{\mu_0}}\frac{n_p}{cos\theta_p} \quad \text{for TM mode} \tag{4b}$$

where μ_0 and ε_0 denote the free space permeability and permittivity respectively. The characteristic matrix for the entire structure can be expressed as,

$$M = \begin{bmatrix} M_{11} & M_{12} \\ M_{21} & M_{22} \end{bmatrix} = \left(M_A M_B M_C\right)^N M_{2D} M_{Defect} M_{2D} \left(M_A M_G M_B M_G\right)^N \tag{5}$$

Here, M_A, M_B, M_C and, M_{Defect} denote the characteristics matrix of CaF$_2$, PtSe$_2$, ZnSe and defect layer respectively. M_{2D} is the characteristics matrix of the WS$_2$ / MoS$_2$ / graphene layer. The elements of the matrix obtained in the above equations can be used to compute transmittance coefficient and reflection coefficient (Panda and Pukhrambam 2021), which can be specified as,

$$t = \frac{2\Psi_0}{\left(M_{11} + M_{12}\Psi_1\right)\Psi_0 + \left(M_{21} + M_{22}\Psi_1\right)} \tag{6}$$

$$r = \frac{\left(M_{11} + M_{12}\Psi_1\right)\Psi_0 - \left(M_{21} + M_{22}\Psi_1\right)}{\left(M_{11} + M_{12}\Psi_1\right)\Psi_0 + \left(M_{21} + M_{22}\Psi_1\right)} \tag{7}$$

where $\Psi_0 = \sqrt{\mu_0/\varepsilon_0}n_0 cos\theta_0$ and $\Psi_s = \sqrt{\mu_0/\varepsilon_0}n_s cos\theta_s$. Here, n_0 and n_s are the refractive index of the air and substrate respectively.

Finally, transmittance (T) and reflectance (R) of the entire structure are computes as,

$$T = \frac{\Psi_1}{\Psi_0}\left|t^2\right| \quad and \quad R = |r|^2 \tag{8}$$

Absorption (A) of the multilayer structure can be given as,

$$A = 1 - T - R \tag{9}$$

As, we observed that the refractive index plays a vital role in the computation of the transfer matrix of each layer. The refractive index of different dielectric layers can be obtained from the Sellmeier equations (https://refractiveindex.info/?shelf=main&book=CaF2&page=Malitson; https://refractiveindex.info/?shelf=main&book=ZnSe&page=Marple), which are stated as follows,

$$n_{CaF2}^2 = 1 + \frac{0.5675888\lambda^2}{\lambda^2 - 0.0050263605^2} + \frac{0.4710914\lambda^2}{\lambda^2 - 0.1003909^2} + \frac{3.8484723\lambda^2}{\lambda^2 - 34.649040^2} \quad (10)$$

$$n_{ZnSe}^2 = 4 + \frac{1.90\lambda^2}{\lambda^2 - 0.113} \quad (11)$$

The dielectric function of monolayer of MoS_2 and WS_2 can be obtained by fitting with multi-Lorentzian function, which is given as (Gan, 2019),

$$\varepsilon(E) = 1 + \sum_{i=1}^{N} \frac{f_i}{E_i^2 - E^2 - jE\rho_i} \quad (12)$$

where E signifies the energy of the photon particle, which is given as $(eV) = \frac{1.2398}{\lambda(\mu m)}$, the model parameters f_i, E_i and ρ_i represent the oscillation strength, resonance energy and spectral width of ith oscillation respectively. The value of f_i, E_i and ρ_i can be determined from the experimental data presented in the reference (Kravets, 2017).

The wavelength dependent refractive index of graphene nanolayer can be computed as given below (Lin and Chen 2019),

$$n_{graphene} = 3 + i\left(\frac{C_1}{3}\right) \times \lambda \quad (13)$$

where C_1 is constant, which is nearly equal to 5.446 μm^{-1} and λ denotes the wavelength of the incident light.

3.1 Sensor performance

Sensitivity (S) is the vital parameter to evaluate the sensor performance. Sensitivity is defined as the ratio of change in resonant wavelength ($\Delta\lambda_{res}$) to the change in RI (Δn) between different blood components, and can be expressed as (Panda et al. 2021),

$$S(nm/RIU) = \frac{\Delta\lambda_{res}}{\Delta n} \quad (14)$$

SNR is defined as the ratio of shift in resonant peak wavelength ($\Delta\lambda_{res}$) to the spectral half-width of the transmission dip ($\Delta\lambda_{1/2}$). Detection limit is signified as the smallest refractive index variation that can be accurately detected by the sensor, whereas resolution of a sensor is defined as the smallest spectral shift, which can be quantified with high accuracy. FOM is the capability of the sensor to sense any small variations in the resonance peak. The aforesaid sensing parameters can be expressed numerically as below (Aly et al. 2020a; Nouman et al. 2020; Panda and Pukhrambam 2021),

$$SNR = \frac{\Delta \lambda_{res}}{\Delta \lambda_{1/2}} \tag{15}$$

$$FOM = \frac{S}{\Delta \lambda_{1/2}} \tag{16}$$

$$Quality\,factor = \frac{\lambda_{res}}{FWHM} \tag{17}$$

$$R = \frac{\Delta \lambda_{1/2}}{1.5 \times SNR^{1/4}} \tag{18}$$

$$DL = \frac{R}{S}. \tag{19}$$

4 Results and discussions

The keystone of the present research is the study of transmission spectrum of the proposed defective 1D structure by employing TMM technique. The resonant modes or defect modes, formed within the PBG, are investigated for different components of blood like plasma, RBC, biotin, serum albumin. We discretely investigated the shift in resonant mode wavelength by separately coating the wall of the defect layer with graphene, MoS_2 and WS_2. The structure parameters like defect layer thickness (d_D) and angle of incidence (θ_i) are properly optimized. The transmittance characteristic is analysed for $d_D = 400$ nm and 500 nm, whereas θ_i is selected as 20° and 40°. For higher values of d_D and θ_i, it is observed that more than one defect modes are formed within the PBG and the intensity of the defect modes are decreased, which makes the analysis difficult and bestows poor performance. So, we restricted our analysis only to $d_D = 400$ nm and 500 nm, and $\theta_i = 20°$ and $40°$.

Figure 2 depicts the transmission spectra of the proposed 1D structure by infiltrating the defect layer with various blood components at different defect layer thickness of 400 nm and 500 nm. This analysis is performed separately by coating the structure with novel 2D materials like WS_2, MoS_2 and graphene. Here, it is observed that, with an increase in refractive index of the blood components, the resonant peak formed within the transmission spectrum is shifted towards higher wavelength. This red-shift phenomenon of defect mode wavelength takes place according to the standing wave condition (Zeng et al. 2014),

$$\sigma = m\lambda = n_{eff}\rho \tag{20}$$

where σ and ρ represent the optical path difference and geometrical path difference respectively, λ denotes the wavelength of the incident light, m is an integer and n_{eff} is the effective refractive index of the proposed structure. Upon infiltrating the defect layer with different blood components, n_{eff} of the defect layer increases, which leads to red-shift in the wavelength, such that σ remains fixed. Additionally, it is perceived that for an increase in defect layer thickness, the resonant peak is red shifted within the PBG. Further, we observed that in case of graphene based sensor configuration, resonant peaks are envisaged at higher wavelengths as compared to WS_2 and MoS_2 based sensor configuration.
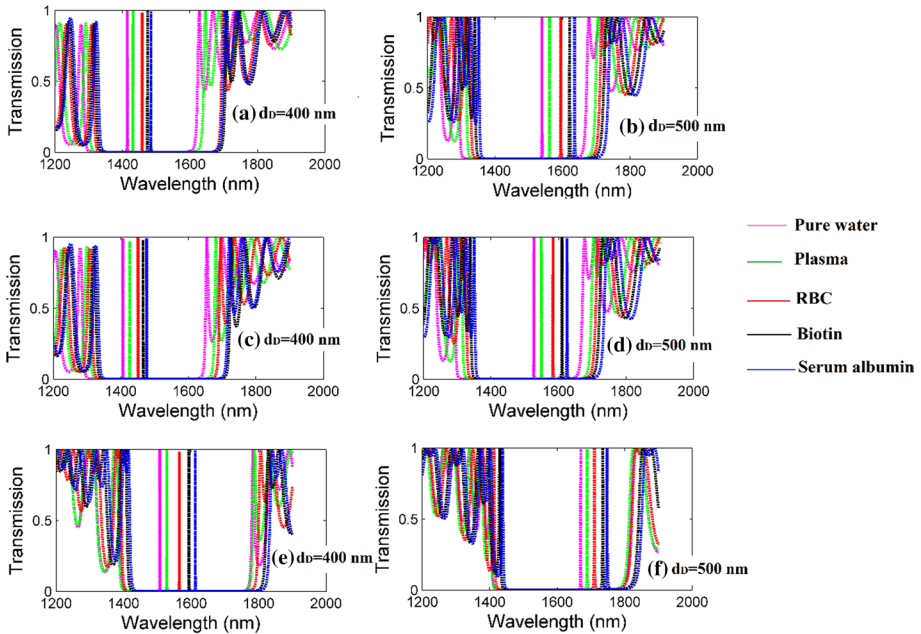
Fig. 2 Transmission spectra of the proposed sensor at $\theta_i = 0°$. **a** WS_2. **b** MoS_2. **c** graphene

We investigated the nature of variation in the wavelength of the resonant peaks of different blood components for all the three shorts of proposed configurations. The position of resonant mode or defect mode depends upon the defect layer thickness and refractive index of the analyte. In Fig. 3, shift in the resonant wavelength is plotted along the primary vertical axis for $d_D = 400$ nm, whereas the same for $d_D = 500$ nm is plotted along the secondary vertical axis in the reverse order. From this figure it is evident that with an increase in the refractive index of the blood components, resonant wavelength increases linearly. Also, it can be observed that for $d_D = 500$ nm, resonant mode is attained at high wavelengths as compared to the case for $d_D = 400$ nm in all the three proposed configurations. It is revealed that for the graphene based structure, resonant modes are formed at higher wavelengths than WS_2 and MoS_2 based structures.

Sensitivity of different blood components at defect layer thickness of 400 nm and 500 nm is inspected for all the proposed configurations, which is shown in Fig. 4. It can be observed that the sensor shows higher sensitivity at $d_D = 500$ nm for both WS_2 and MoS_2 based structure, whereas a deviation is noticed at graphene based proposed sensor. As it can be seen, for graphene based 1D structure, high sensitivity is attained at $d_D = 400$ nm than $d_D = 500$ nm. On comparing the aforementioned three types of structure configurations, it is perceived that optimum sensitivity of 1100.23 nm/RIU is achieved for WS_2 based sensor configuration at $d_D = 500$ nm.

Further, the effect of number of layers (L) of the proposed 2D materials (WS_2, MoS_2, graphene) on the transmission characteristics is thoroughly scrutinized at $d_D = 500$ nm by considering plasma (n = 1.35) in the defect layer, which is delineated in Fig. 5. Interestingly, it is realized that with an increase in number of layers, the position of the defect mode is red-shifted (i.e. moves towards higher wavelengths), whereas the intensity of the resonant mode decreases drastically. With increase in the value of L, the overall thickness
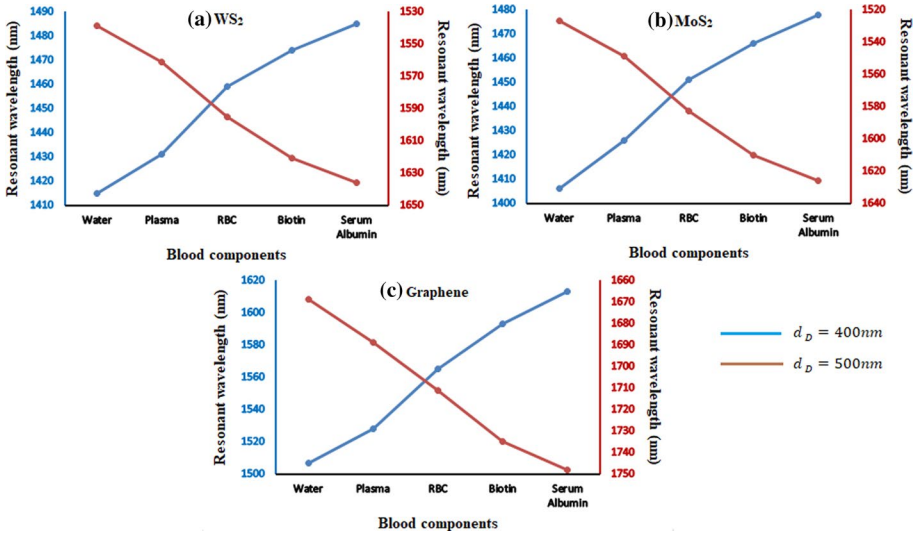
Fig. 3 Shift in the resonant wavelength of the proposed structures at different defect layer thickness. **a** WS_2. **b** MoS_2. **c** graphene
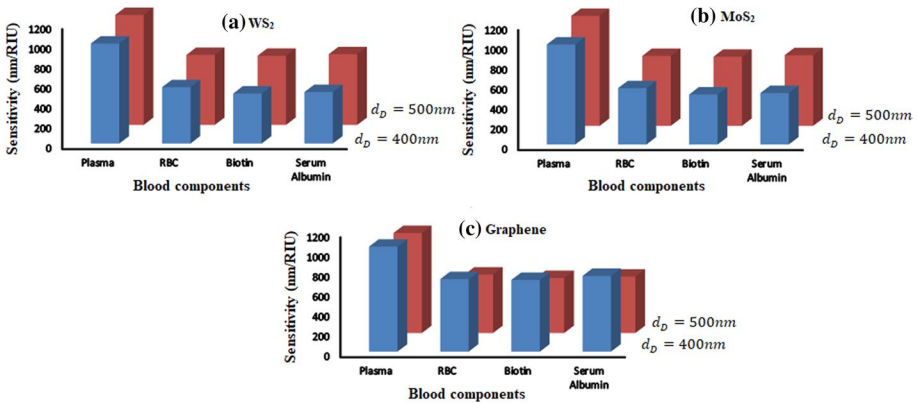

Fig. 4 Sensitivity at different defect layer thickness at $\theta_i = 0°$. **a** WS_2. **b** MoS_2. **c** graphene configurations
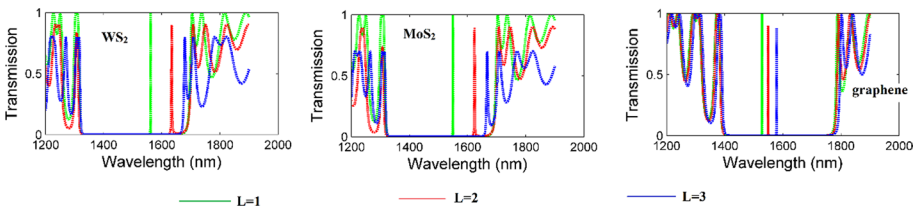

Fig. 5 Transmission spectra of the proposed structure configurations for different number of layers of 2D materials. **a** WS_2. **b** MoS_2. **c** graphene at $d_D = 500$ nm, n = 1.35

of the 1D PhC structure increases as explained in the Sect. 2, which leads to increase in the geometrical path difference (ρ). So, according to Eq. (20), with increase in ρ, the wavelength shifts towards longer wavelength (i.e. red-shift) at a constant m and n_{eff}. Moreover, it is envisaged that for higher number of layers, the FWHM (full width half maximum) of the resonant mode increases, which will reduce the sensor performance, i.e. high value of FWHM leads to reduction in signal-to-noise ratio, figure of merit and quality factor. Thus, to achieve high performance we selected monolayer (L = 1) of WS$_2$, MoS$_2$ and graphene in all the analysis presented in this research.

As we observed a high sensitivity at defect layer thickness of 500 nm, so we fixed this thickness value and investigated the transmittance spectrum under variable incidence angles ($\theta_i = 20°, 40°$) of the EM signal, which is depicted in Fig. 6. The defect mode properties such as spectral position, FWHM and intensity undergo considerable change with change in the incidence angle. In particular, it is observed that the defect mode position is blue-shifted (i.e. moved towards lower wavelengths) for increase in θ_i. The main cause for this blue-shift in wavelength can be explained by the Bragg condition, which is given as (Aly et al. 2020b),

$$m\lambda_{res} = 2N\sqrt{n_{eff}^2 - sin^2\theta_i} \qquad (21)$$

where λ_{res} is the defect mode wavelength, m represents the constructive diffraction order, θ_i denotes the angle of incidence, n_{eff} indicates effective refractive index of the multilayers, and N signifies the period of dielectric layers. So, with an increase in θ_i, the defect mode wavelength is blue-shifted, to satisfy Bragg condition. Also, the aforementioned behavior is observed in the researches cited in the literature (Aly et al. 2020a; Jahania et al. 2020; Shaban et al. 2020; Bouzidi et al. 2017; Abd El-Aziz et al. 2019b; Nouman et al. 2020).
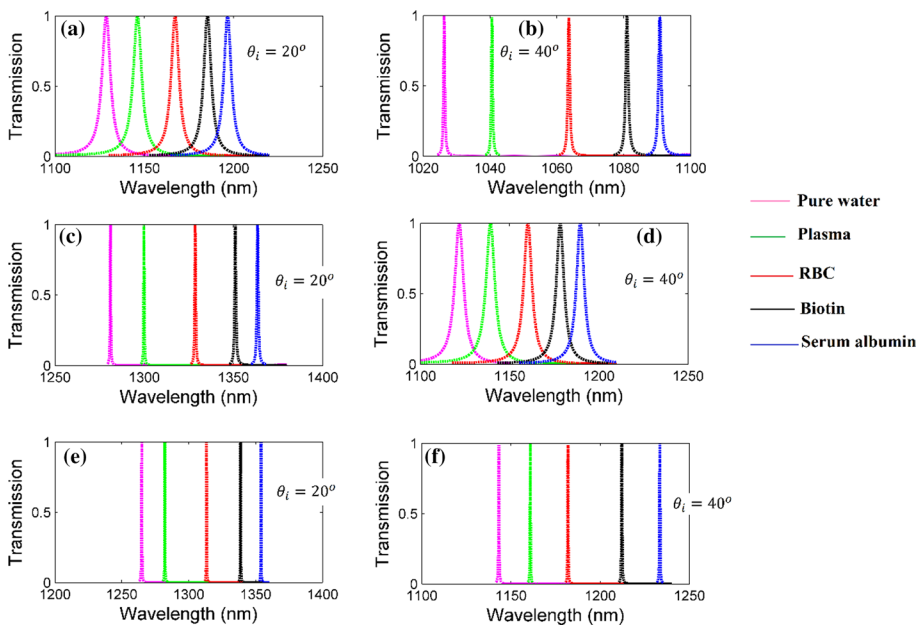

Fig. 6 Transmittance spectrum of the proposed sensors at different angles of incidence for **a**, **b** WS$_2$, **c**, **d** MoS$_2$, **e**, **f** graphene
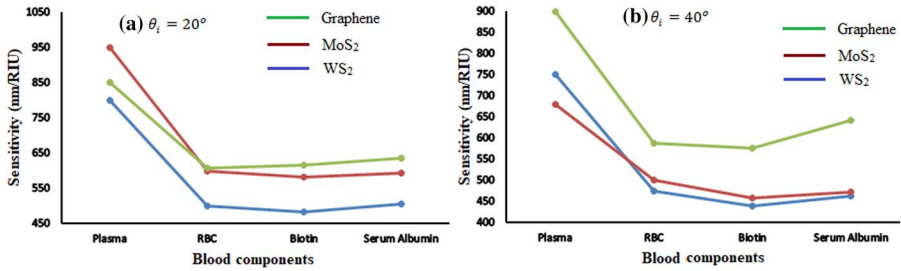
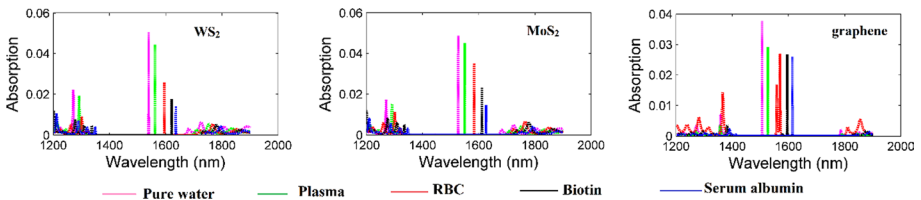**Fig. 7** Sensitivity of the proposed structures at different incident angles of $\theta_i = 20°$, $40°$

Fig. 8 Absorption spectrum of the proposed structures for blood components at $d_D = 500$ nm and $\theta_i = 0°$

We also numerically studied the sensitivity of the proposed structures at different incident angles of 20° and 40° at $d_D = 500$ nm, which is shown in Fig. 7. It is found that the variation in the sensitivity for different blood components shows a nonlinear trend. If we compare the sensitivity for different incident angles ($\theta_i = 0°$, 20°, 40°), it can be clearly observed that the proposed structures show maximum sensitivity at $\theta_i = 0°$ (shown in Fig. 4).

The absorption spectrum for all the three proposed configurations is shown in Fig. 8. From Fig. 2, we have already verified that intensity of transmission spectra are above 95% for different blood components. So, here in Fig. 8, it is apparent that intensity of the absorption spectra are very small, less than 5%. Further, it is observed that intensity of the absorption spectra are decreased and red-shifted with increase in the refractive index of different blood components.

We also studied the absorption spectrum of the WS_2 based sensor configuration by considering plasma as the infiltrated blood component at different angles of incidence at $d_D = 500$ nm, which is delineated in Fig. 9. Here, it is perceived that absorption spectrum is blue-shifted with increase in the angle of incidence and the intensity of absorption is relatively more at higher incident angle.

Figure 10 shows the transmission spectrum of the proposed WS_2 based defective 1D PhC under infiltrating the defect layer with plasma. To select the optimum value of N, we carried out the above said analysis for different number of period (N) i.e. N = 3, 5, 7, 9. From Fig. 10, it is evident that in case of N = 3, the FWHM of the transmission spectrum is very large, thus the structure will show poor sensing performance. For N = 5, 7, 9, although the position of the resonant mode is nearly same, but intensity of the resonant mode decreases drastically with increase in the value of N. To accomplish optimum sensing performance, the intensity of the resonant mode should be high, so we selected N = 5, where high transmittance intensity of nearly 95% is achieved.
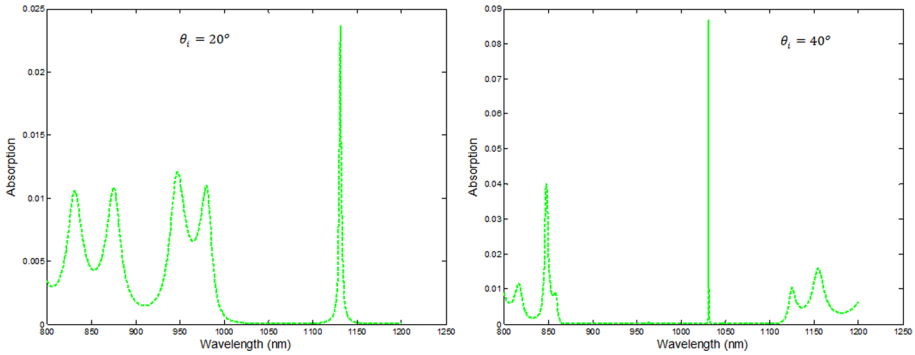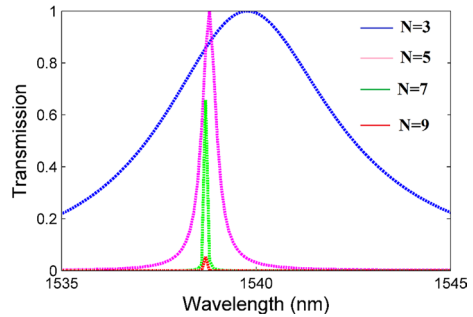
Fig. 9 Absorption spectrum of the WS_2 based sensor for blood plasma at $d_D = 500$ nm

Fig. 10 Transmittance spectrum for different number of period (N)

Variation in SNR with respect to different blood components, of the proposed sensor designed with WS_2, MoS_2 and graphene material, is represented in Fig. 11. Here, the primary vertical axis shows the SNR variation for $d_D = 400$ nm, whereas the secondary vertical axis is meant for SNR variation for $d_D = 500$ nm, where data are plotted in reverse order. It can be perceived that SNR increases with increase in the refractive index of the different blood components. Also, it is revealed that higher value of SNR is noticed at $d_D = 500$ nm for WS_2 and MoS_2 based structures, but on the contrary maximum SNR is obtained at $d_D = 400$ nm for graphene based sensor configuration.

We studied the FOM of the proposed sensor configurations at different defect layer thickness, which is delineated in the Fig. 12. Unlike SNR, variation in FOM for different blood constituents follows a nonlinear trend. A higher FOM is perceived at $d_D = 500$ nm as compared to $d_D = 400$ nm.

Variation in the quality factor (Q) of the proposed structures is shown in Fig. 13 at different defect layer thickness. Here, it is asserted that quality factor in order of 10^3 is obtained, which indicates the proposed sensor delivers excellent sensing characteristics. Additionally, it is clearly observed that a higher Q value is obtained at $d_D = 500$ nm as compared to $d_D = 400$ nm.

Figure 14 represents the variation in resolution and detection limit (DL) of the proposed sensors with respect to different blood components. Resolution in nm is plotted along the primary vertical axis, whereas DL in RIU is taken along the secondary vertical axis in reverse order. It is observed that a very low resolution is obtained for $d_D = 500$ nm for
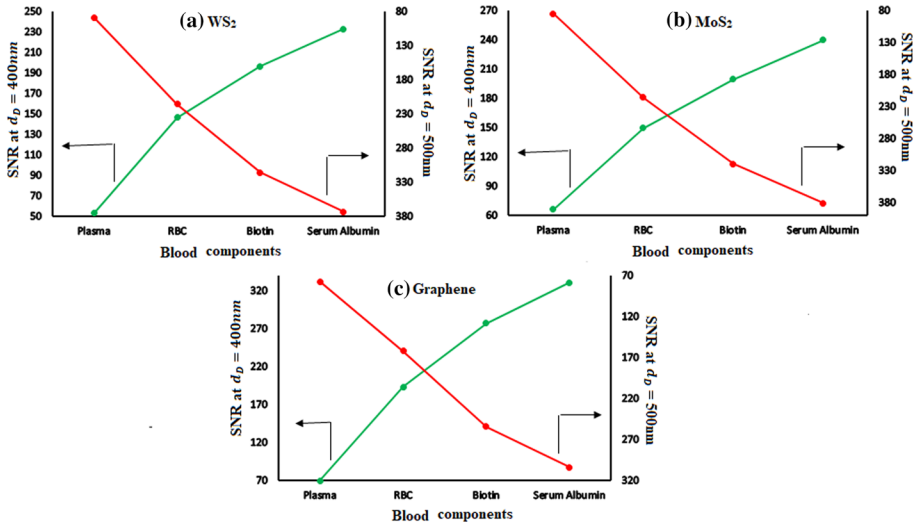
Fig. 11 SNR of the proposed sensor for different defect layer thickness. **a** WS_2. **b** MoS_2. **c** graphene based configuration
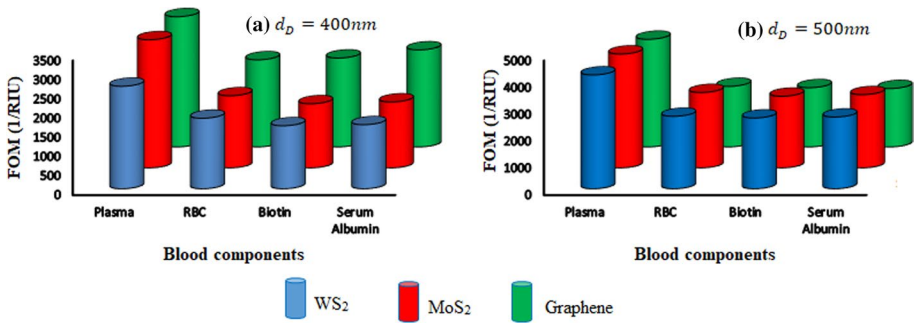

Fig. 12 FOM of the proposed sensors at different defect layer thickness

different proposed sensor configurations. Similarly, a very low DL in the order of 10^{-5} is attained for $d_D = 500$ nm. Such minimal value of resolution and DL indicate that high performance characteristics can be achieved with the proposed sensor configurations. Finally, optimum value of sensing parameters (maximum SNR, QF, FOM and minimum R, DL) for the three different sensor configurations are listed in Table 1.
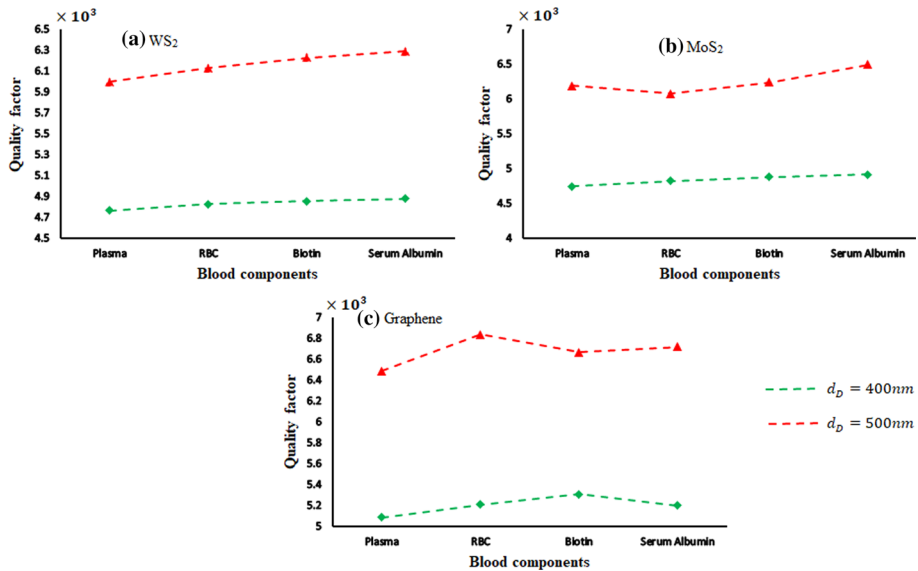
Fig. 13 Quality factor of the proposed structures at different defect layer thickness

5 Conclusions

We propose a novel 1D defective PhC, which employs completely new combination of materials like CaF_2, $PtSe_2$ and ZnSe, for real-time and label-free detection of different blood components such as plasma, RBC, biotin, serum albumin. The wall of defect layer is separately coated with novel 2D materials like WS_2, MoS_2 and graphene, which is further infiltrated with different blood components. TMM is manipulated in the proposed structure to analyse its transmission and absorption spectrum. Different geometrical parameters like thickness of dielectric layers, thickness of defect layer, thickness of 2D materials, period of the dielectric layers, incident angle are properly optimized to attain high intensity and low FWHM resonant mode, formed within the PBG in the transmission spectrum. By studying the shift in resonant mode wavelength with respect to various blood components, we evaluated different performance measuring parameter of the proposed sensors like sensitivity, SNR, QF, FOM, resolution and DL. From the outcomes, it is observed that all the three sensor configurations show optimum sensing performance at $d_D = 500$ nm and $\theta_i = 0°$. Moreover, with the available simple and cost effective fabrication techniques, the proposed sensors open up an avenue for future advancement in the biosensing research field.
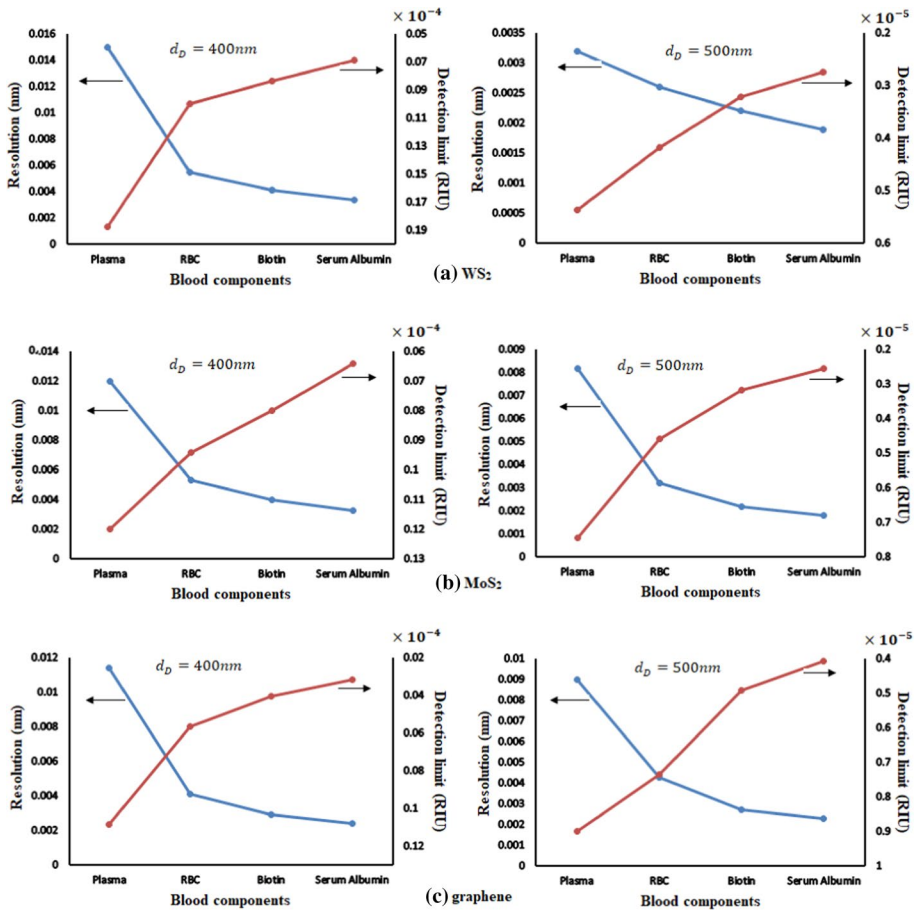
Fig. 14 Resolution and detection limit of the proposed sensors at different defect layer thickness

Table 1 Optimum value of sensing parameters

Proposed sensor configurations	S (nm/RIU)	SNR	FOM (1/RIU)	QF	R (nm)	DL (RIU)
$(CaF_2/PtSe_2/ZnSe/ PtSe_2)^5$ $(WS_2/D/WS_2)$ $(CaF_2/PtSe_2/ZnSe/ PtSe_2)^5$	1100.23	373.07	4230.76	6.29×10^3	0.0019	0.27×10^{-5}
$(CaF_2/PtSe_2/ZnSe/ PtSe_2)^5$ $(MoS_2/D/MoS_2)$ $(CaF_2/PtSe_2/ZnSe/ PtSe_2)^5$	1092.5	380.76	4227.51	6.5×10^3	0.0018	0.25×10^{-5}
$(CaF_2/PtSe_2/ZnSe/ PtSe_2)^5$ $(Graphene/D/Graphene)(CaF_2/ PtSe_2/ZnSe/ PtSe_2)^5$	1050	331.25	4000	6.84×10^3	0.0023	0.40×10^{-5}

Availability of data and material Not applicable.Code availability Not applicable.

Declarations

Conflicts of interest There is no conflict of interest.

References

Abd El-Aziz, O.A., Elsayed, H.A., Sayed, M.I.: One-dimensional defective photonic crystals for the sensing and detection of protein. Appl Opt. **58**(30), 8309–8315 (2019a)

Abd El-Aziz, O.A., Elsayed, H.A., Sayed, M.I.: One-dimensional defective photonic crystals for the sensing and detection of protein. Appl. Opt. **58**(30), 8309–8315 (2019b)

Ahmed, A.M., Mehaney, A.: Ultra-high sensitive 1D porous silicon photonic crystal sensor based on the coupling of Tamm/Fano resonances in the mid-infrared region. Sci. Rep. **9**, 6973 (2019). https://doi.org/10.1038/s41598-019-43440-y

Aly, A.H., Sayed, F.A.: THz cutoff frequency and multifunction $Ti_2Ba_2Ca_2Cu_3O_{10}$/GaAs photonic bandgap materials. Int. J. Mod. Phys. B **34**(10), 2050091 (2020). https://doi.org/10.1142/S0217979220500915

Aly, A.H., et al.: Biophotonic sensor for the detection of creatinine concentration in blood serum based on 1D photonic crystal. RSC Adv. **10**, 31765–31772 (2020a)

Aly, H.A., et al.: Theoretical study of hybrid multifunctional one-dimensional photonic crystal as a flexible blood sugar sensor. Phys. Scr. **95**, 035510 (2020b). https://doi.org/10.1088/1402-4896/ab53f5

Arunkumar, R., Suaganya, T., Robinson, S.: Design and analysis of 2D photonic crystal based biosensor to detect different blood components. Photonic Sens. **9**, 69–77 (2019)

Boedecker, G., Henkel, C.: All-frequency effective medium theory of a photonic crystal. Opt. Express **11**, 1590–1595 (2003). https://doi.org/10.1364/OE.11.001590

Bonaccorso, F., Sun, Z., Hasan, T., Ferrari, A.C.: Graphene photonics and optoelectronics. Nat. Photonics **4**, 611–622 (2010)

Bouzidi, A., Bria, D., Falyouni, F., Akjouj, A., Lévêque, G., Azizi, M., Berkhli, H.: A biosensor based on one-dimensional photonic crystal for monitoring blood glycemia. J. Mater. Environ. Sci. **8**(11), 3892–3896 (2017)

Boyd, R.W., Heebner, J.E.: Sensitive disk resonator photonic biosensor. Appl. Opt. **18**(31), 15742–15747 (2001)

Chen, H.L., Lee, H.F., Chao, W.C., Hsieh, C.I., Ko, F.H.: Fabrication of autocloned photonic crystals by using high-density-plasma chemical vapor deposition. Vac. Sci. Technol. B **22**, 3359 (2008)

Devashish, D., Ojambati, O.S., Hasan, S.B., van der Vegt, J.J.W., Vos, W.L.: Three-dimensional photonic band gap cavity with finite support: enhanced energy density and optical absorption. Phys. Rev. B **99**, 075112 (2019). https://doi.org/10.1103/PhysRevB.99.075112

Elsayed, H.A.: A multi-channel optical filter by means of one dimensional n doped semiconductor dielectric photonic crystals. Mater. Chem. Phys. **216**, 191–196 (2018)

Entezar, S.R., Saleki, Z., Madani, A.: Optical properties of a defective one-dimensional photonic crystal containing graphene nano layers. Phys. B **478**, 122–126 (2015)

Falkovsky, L.A., Pershoguba, S.S.: Optical far-infrared properties of a graphene mono layer and multilayer. Phys. Rev. B **76**(15), 153410 (2007). https://doi.org/10.1103/PhysRevB.76.153410

Gan, S., et al.: Ultra-sensitive refractive index sensors based on Bloch surface waves with transition metal dichalcogenides. IEEE Sens. J. **19**(19), 8675–8680 (2019)

Geim, A.K.: Graphene: status and prospects. Science **324**, 1530–1534 (2009)

Ghasemi, F., Entezar, S.R., Razi, S.: Terahertz tunable photonic crystal optical filter containing graphene and nonlinear electro-optic polymer. Laser Phys. **29**, 056201 (2019). https://doi.org/10.1088/1555-6611/ab05c2

Guo, Y., et al.: Two-dimensional PtSe2 theoretically enhanced Goos–Hänchen shift sensitive plasmonic biosensors. Plasmonics **15**, 1815–1826 (2020)

Han, L., et al.: Comprehensive study of SPR biosensor performance based on metal-ITO-graphene/TMDC hybrid multilayer. Plasmonics **14**, 2021–2030 (2019)

Hattori, T.: Third-order nonlinearity enhancement in one-dimensional photonic crystal structures. Jpn. J. Appl. Phys. **41**, 1349–1353 (2002)

Hemmatyar, O., Rahmani, B., Bagheri, A., Khavasi, A.: Phase resonance tuning and multi-band absorption via graphene-covered compound metallic gratings. IEEE J. Quantum Electron. **53**, 1–10 (2017)

https://refractiveindex.info/?shelf=main&book=CaF2&page=Malitson

https://refractiveindex.info/?shelf=main&book=ZnSe&page=Marple.

Ilinykh, V.A., Matyushkin, L.B.: Sol-gel fabrication of one-dimensional photonic crystals with predicted transmission spectra. J. Phys. Conf. Ser. **741**, 012008 (2016). https://doi.org/10.1088/1742-6596/741/1/012008

Jahania, D., Raissi, B., Taati, F., Riahifar, R., Yaghmaee, M.S.: Optical properties of fluidic defect states in one-dimensional graphene-based photonic crystal biosensors: visible and infrared Hall regime sensing. Eur. Phys. J. plus. **135**, 160 (2020). https://doi.org/10.1140/epjp/s13360-019-00056-5

Janisch, C., et al.: Extraordinary second harmonic generation in tungsten disulfide monolayers. Sci. Rep. **4**(1), 5530 (2015). https://doi.org/10.1038/srep05530

Jia, Y., Li, Z., Wang, H., Saeed, M., Cai, H.: Sensitivity enhancement of a surface plasmon resonance sensor with platinum diselenide. Sensors **20**(1), 131 (2020)

John, S.: Strong localization of photons in certain disordered dielectric superlattices. Phys. Rev. Lett. **58**, 2486–2489 (1987)

Keshavarz, A., Zangenehzadeh, S., Hatef, A.: Optimization of surface plasmon resonance-based biosensors for monitoring hemoglobin levels in human blood. Appl. Nanosci. **10**, 1465–1474 (2020)

Kravets, V.G., et al.: Ellipsometry and optical spectroscopy of low-dimensional family TMDs. Semicond. Phys. Quantum Electron. Optoelectron. **20**(3), 284–296 (2017)

Kukkar, M., Sharma, A., Kumar, P., Kim, K.H., Deep, A.: Application of MoS2 modified screen printed electrodes for highly sensitive detection of bovineserum albumin. Anal. Chim. Acta **939**, 101–107 (2016)

Lin, C., Chen, S.: Design of high-performance Au-Ag-dielectric graphene based surface plasmon resonance biosensors using genetic algorithm. J. Appl. Phys. **125**, 113101 (2019). https://doi.org/10.1063/1.5066354

Liu, X., et al.: Enhanced X-ray photon response in solution-synthesized CsPbBr3 nanoparticles wrapped by reduced graphene oxide. Sol. Energy Mater. Sol. Cells **187**, 249–254 (2018)

Mittal, V., et al.: Optical quality ZnSe films and low loss waveguides on Si substrates for mid-infrared applications. Opt. Mater. Express **7**(3), 712–725 (2017)

Mohammed, N.A., et al.: High-sensitivity ultra-quality factor and remarkable compact blood components biomedical sensor based on nanocavity coupled photonic crystal. Results Phys. **14**, 102478 (2019). https://doi.org/10.1016/j.rinp.2019.102478

Nouman, W.M., Abd El-Ghany, S.E., Sallam, S.M., Dawood, A.F., Aly, A.H.: Biophotonic sensor for rapid detection of brain lesions using 1D photonic crystal. Opt. Quant. Electron. **52**, 287 (2020). https://doi.org/10.1007/s11082-020-02409-2

Panda, A., Devi, P.P.: Photonic crystal biosensor for refractive index based cancerous cell detection. Opt. Fiber Technol. **54**, 102123 (2020). https://doi.org/10.1016/j.yofte.2019.102123

Panda, A., Pukhrambam, P.D.: Investigation of defect based 1D photonic crystal structure for real-time detection of waterborne bacteria. Phys. B **607**(3), 412854 (2021). https://doi.org/10.1016/j.physb.2021.412854

Panda, A., Sarkar, P., Palai, G.: Research on SAD-PRD losses in semiconductor waveguide for application in photonic integrated circuits. Optik **154**, 748–754 (2018)

Panda, A., Pukhrambam, P.D., Keiser, G.: Realization of sucrose sensor using 1D photonic crystal structure vis-à-vis band gap analysis. Microsyst. Technol. **27**, 833–842 (2021)

Qi, H., Wang, L., Sun, J., Long, Y., Hu, P., Liu, F., He, X.: Production methods of vander waals hetero structures based on transition metal dichalcogenides. Curr. Comput.-Aided Drug Des. **8**(1), 35 (2018). https://doi.org/10.3390/cryst8010035

Schürmann, U., Takele, H., Zaporojtchenko, V., Faupel, F.: Optical and electrical properties of polymer metal nanocomposites prepared by magnetron co-sputtering. Thin Solid Films **515**, 801–804 (2006)

Shaban, S.M., Mehaney, A., Aly, A.H.: Determination of 1-propanol, ethanol and methanol concentrations in water based on 1D phoxonic crystal sensor. Appl. Opt. **59**(13), 3878–3885 (2020)

Sharma, P., et al.: Design and simulation of photonic crystal based biosensor for detection of different blood components. In: 2014 IEEE Region 10 Symposium, Kuala Lumpur, pp. 171–176 (2014). https://doi.org/10.1109/TENCONSpring.2014.6863019

Shi, B., Jiang, Z.M., Wang, X.: Defective photonic crystals with greatly enhanced second-harmonic generation. Opt. Lett. **26**, 1194–1196 (2001)

Wang, H., Yan, K.P., Xie, J., Duan, M.: Fabrication of ZnO colloidal photonic crystal by spin-coating method. Mater. Sci. Semicond. Process. **11**(2), 44–47 (2008)

Wang, Y., et al.: Monolayer PtSe2, a new semiconducting transition-metal dichalcogenide, epitaxially grown by direct selenization of Pt. Nano Lett. **15**, 4013–4018 (2015)

Wei, J., et al.: Enhanced performance of light-controlled conductive switching in hybrid cuprous oxide/reduced graphene oxide (Cu2O/rGO) nanocomposites. Opt. Lett. **42**(5), 911–914 (2017)

White, I.M., Fan, X.: On the performance quantification of resonant refractive index sensors. Opt. Express **16**(2), 1020–1028 (2008)

Wolf, D.J., Zitelli, J.A.: Surgical margins for basal cell carcinoma. Arch. Dermatol. **123**(3), 340344 (1987). https://doi.org/10.7759/cureus.9211

Yablanovitch, E.: Inhibited spontaneous emission in solid state physics and electronics. Phys. Rev. Lett. **58**, 2059–2062 (1987)

Yuan, L., Huang, L.: Exciton dynamics and annihilation in WS2 2D semiconductors. Nanoscale **7**, 7402–7408 (2015)

Zahid, M.A., et al.: Optical properties of CaF2 thin film deposited on borosilicate glass and its electrical performance in PV module applications. Appl. Sci. **10**, 5647 (2020). https://doi.org/10.3390/app10165647

Zang, Z., et al.: Tunable photoluminescence of water-soluble AgInZnS–graphene oxide (GO) nanocomposites and their application in-vivo bioimaging. Sens. Actuators B Chem. **252**, 1179–1186 (2017)

Zeng, C., Luo, C., Hao, L., Xie, Y.: The research on magnetic tunable characteristics of photonic crystal defect localized modes with a defect layer of nanoparticle. Chin. Opt. Lett. **12**, 11602 (2014). https://doi.org/10.3788/COL201412.S11602

Zhu, B., Chen, X., Cui, X.: Exciton binding energy of monolayer WS2. Sci. Rep. **5**, 9218 (2015). https://doi.org/10.1038/srep09218